

Synthesis of Amine-Stabilized Aqueous Colloidal Iron Oxide Nanoparticles

M. Aslam,[†] Elise A. Schultz,[‡] Tao Sun[†] Thomas Meade,[‡] and Vinayak P. Dravid^{*†}

Department of Materials Science and Engineering and the International Institute for Nanotechnology, and Department of Chemistry and Department of Biochemistry and Molecular and Cell Biology, Neurobiology and Physiology, Feinberg School of Medicine, Northwestern University, 2145 Sheridan Road, Evanston, Illinois 60208

Received September 29, 2006; Revised Manuscript Received January 17, 2007

ABSTRACT: We demonstrate a simple one-step process for the synthesis of iron oxide nanoparticle aqueous colloids using the multifunctional molecule dodecylamine (DDA), which electrostatically complexes with aqueous iron ions (one precursor Fe^{2+} from FeCl_2), reduces them, and subsequently caps the nanoparticles. The iron oxide particles thus synthesized are of the face-centered cubic (FCC) phase with a high degree of monodispersity and an appropriate concentration of the amine-capping molecular layer. The aqueous magnetic nanocrystalline colloids were characterized by TEM, XRD, XPS, TGA/DTA, and FTIR spectroscopy techniques. The relaxivity, stability, and hydrodynamic size of the nanoparticles were investigated for potential application in magnetic resonance imaging (MRI). The magnetic properties were also studied by using a superconducting quantum interference device (SQUID) magnetometer at room temperature. We believe that such a simple one-step synthesis of biocompatible aqueous nanomagnetic colloids will have viable applications in biomedical imaging, diagnostics, and therapeutics.

Iron oxide is one of the most popular multifunctional magnetic materials with diverse applications including multi-tera bit storage device,^{1–3} catalysis,^{4,5} sensors,⁶ and a platform for high-sensitivity biomolecular magnetic resonance imaging (MRI) for medical diagnosis and therapeutics.^{7–10} One of the main shortcomings of conventionally synthesized and polymer-functionalized Fe_3O_4 for biomedical applications is the presence of a thick polymer layer that increases the hydrodynamic radii considerably (up to 100 nm), causing the dampening of the MR signal. Introduction of a cationic surface layer with (NH_2) amine on top of iron oxide nanoparticles surface is believed to have very good uptake by the cancer cells and provide sharper in vitro and in vivo MRI signals as compared to the conventional cross-linked iron oxide (CLIO) nanoparticles.^{9,10} However, it is not clear if these nanoparticles will have better biostability (including buffer saline, different pH conditions) with higher loading and enhanced biocompatibility and optimal magnetism as compared to dextran-coated CLIO nanoparticles; hence, the need is to optimize surface functionality of these magnetic particles to create a versatile platform for variety of biomedical and bioclinical applications.

Iron oxide colloidal suspensions with discrete size deviation and a superparamagnetic behavior (size regime of 5–20 nm) are now envisioned as building blocks for many biomedical applications. Several approaches have been developed to synthesize Fe_3O_4 nanoparticles. However, compared to the well-known alkaline oxidation route,¹¹ which is believed to not be suitable for many in vivo applications, the more promising routes are thermal decomposition of various organometallic iron precursors. For example, very recently, Sun et al.¹² reported highly uniform magnetite nanoparticles through Fe–acetylacetonate decomposition in phenyl ether; the most promising route for large-scale synthesis of the Fe_3O_4 structure is the Fe–oleate precursor decomposition by annealing at 320 °C in high-boiling-point octadecene.¹³ More recently, a modified synthetic approach in highly polar solvent was proposed by Gao et al.¹⁴ that renders particles water-soluble as opposed to previously mentioned thermal decomposition methods, which require further surface modification to pull organic-soluble particles into water, which results in lower yield and poor dispersion. From the synthesis point of view, an important consideration will be to

prepare nanoparticles economically using relatively low-grade reagents under aerobic conditions. The motivation for our work stems from the need for aqueous synthesis of iron oxide colloidal nanoparticles under ambient conditions.

In this article, we report a one-step aqueous approach to synthesizing Fe_3O_4 nanoparticles from a single FeCl_2 precursor using a long-chain amine (dodecylamine, DDA) as the reducing and surface-functionalizing agent. Capping of iron oxide nanoparticles with the amine molecules stabilizes the particles in solution nearly covalently and renders them water-dispersible. The procedure is reported in the references section.¹⁵ We illustrate through structural characterization that control of amine concentration with respect to Fe^{2+} concentration gives control of the size and morphology of the product. The amine-capped nanoparticles can be obtained in the form of a highly air-stable dry powder after evaporation of the aqueous component that is readily redispersible in water as well as nonaqueous solvents. Amine-group-functionalized Fe_3O_4 nanoparticles may offer an excellent platform for next generation nanobiocomposites and biotracers. As an example, this surface functionality is used for the covalent binding of a fluorescent dye, 4-chloro-7-nitrobenzofurazan (NBD), to the nanoparticles.¹⁶

The core size and size distribution of the amine-stabilized iron oxide nanoparticles were examined by transmission electron microscopy (TEM). Figure 1 shows the TEM images of iron oxide nanoparticles with three different sizes. As the dodecylamine to FeCl_2 molar ratio increased to 1, the particle size increased. The higher the molar ratio was above 3, the smaller the nanoparticles. This trend agreed with that reported in the literature.¹⁷ The inset in Figure 1A is the HRTEM image of corresponding nanoparticles.

Product of reaction 1 (1:1 Fe:amine mole ratio) shows that the nanoparticles consist of two distinct broad size distributions typically in the range of 10–40 nm (Figure 1A). The improved uniformity in particle size distribution in reaction 2 (1:4 Fe:amine mole ratio) and reaction 3 (1:7 Fe:amine mole ratio) is clearly evident from the TEM images of images B and C of Figure 1, respectively. It can be seen that at higher amine concentrations, the particle size becomes more uniform. A closer look at these particles is shown in images E and F of Figure 1, and these images are used to estimate the particle size distribution. Figure 1D shows the particle size distribution plot of about 60 particles for reaction 2 and 150 particles for reaction 3. These plots further corroborate the results from TEM and show that the particle size distribution is much narrower after reaction 2 (1:4 Fe:amine mole ratio) with a standard deviation of within 15% compared to greater than 40% for reaction 1 (1:1 Fe:

* To whom correspondence should be addressed. E-mail: v-dravid@northwestern.edu.

[†] Department of Materials Science and Engineering and the International Institute of Nanotechnology, Northwestern University.

[‡] Department of Chemistry and Department of Biochemistry and Molecular and Cell Biology, Northwestern University.

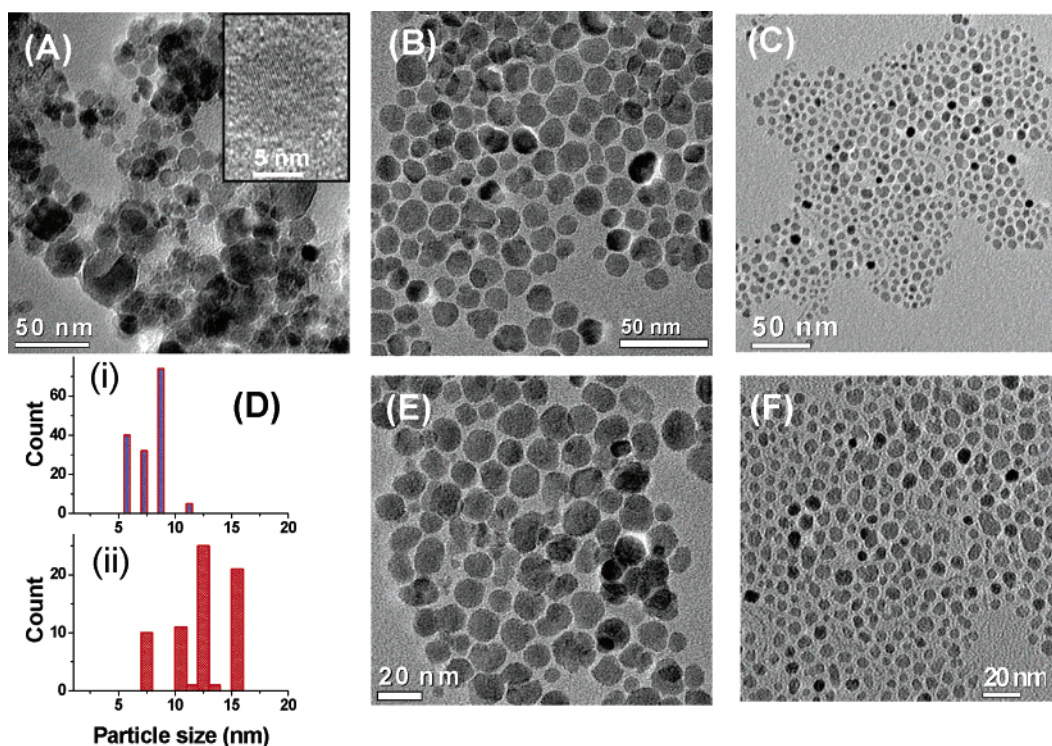


Figure 1. Brigh-field TEM images of iron oxide nanoparticles produced with (A) 1:1 Fe:amine mole ratio (reaction 1), (B) 1:4 Fe:amine mole ratio (reaction 2), and (C) 1:7 Fe:amine mole ratio (reaction 3). Inset of Figure 1A indicates HRTEM image of one iron oxide nanoparticle revealing the lattice fringes. (E, F) Magnified images of samples B and C, respectively. (D) Particle size distribution showing narrower size for (i) 1:7 Fe:amine mole ratio and (ii) size distribution for particles prepared with a 1:4 Fe:amine mole ratio. The size distribution plots are obtained from TEM images E and F by counting nearly 70 and 150 particles.

amine mole ratio). Moreover, the average particle size after reaction 2 is controlled well with respect to amine concentration (13 ± 1 nm and 8.5 ± 1 nm, respectively). The control of core size with respect to amine concentration is similar to the well-known “Au–thiol” system, in which the cores of thiol-stabilized Au nanoparticles decrease in size and dispersity with increasing thiol concentration.¹⁸ This is not surprising, considering that higher amine surfactant concentration would have finer iron oxide particles with narrower size distribution. At present, we understand that there is a simple correlation between amine concentration and particle size. The particle size increases with a decrease in the concentration of DDA.

Although the TEM images demonstrate the uniformity of particles with respect to DDA concentration and the high-resolution images reveal the necessary crystallinity, the Fe_3O_4 phase formation was corroborated by the X-ray diffraction (XRD) patterns. It showed broad peaks assigned to the h^{11} (311), (400), (511), and (440) planes of a face-centered cubic (fcc) lattice of iron oxide (Figure 2 A). The corresponding lattice constant is $a = 0.82$ nm, which matches to the reported standard data (JCPDS file 19-629; $a = 0.8393$ nm). The crystallographic form of Fe_3O_4 nanoparticles was also verified by its structural transformation to maghemite upon oxidation at 300 °C. Noticeable changes in peak positions are shown in Figure 2B, in addition to new peaks that appear after oxidation (please refer to the Supporting Information, Figure S2, for the full XRD spectra of as-synthesized samples annealed at 300 and 600 °C). The resulting patterns after annealing at 300 and 600 °C match well with maghemite and hematite phases, respectively. The average particle size of the nanoparticles (11.9 and 8.2 nm) calculated by the Scherrer formula, using the full width half-maximum (fwhm) of the intense (311) reflection (panels C and D of Figure 2), was comparable with the value obtained from TEM images (reaction 2 and reaction 3, images B and C of Figure 1, respectively). Three different curves in panels C and D of Figure 2 demonstrate the growth kinetics of the nanoparticles after reactions times of 3, 6, and 12 h, whereas XRD patterns in Figure 2E illustrate two distinct particle sizes revealing a sharp peak for the bigger particle size

achieved with lower amine concentration. In addition to concentration, the particle size and distribution were affected by the time variation (see the Supporting Information). For instance, a reaction time of 3 h (see the Supporting Information, images a and b of Figure 1S) afforded irregular shaped nanoparticles with rods ranging from 20 to 30 nm in diameter. After a reaction time of 12 h, the particle size became very large (average diameter 30 ± 10.5 nm) and the particle size distribution was relatively broad (see the Supporting Information, images c and d of Figure 1S). Thus, the particle size and distribution of iron oxide nanoparticles prepared in this work were strongly controlled by the DDA:iron ion molar ratio.

The reaction mechanism of nanoparticle formation from a single precursor Fe^{2+} to Fe_3O_4 is not very well understood. However, on the basis of the results with the amine-based chelation and subsequent reduction, we believe and propose that the reaction mechanism is simple and proceeds with amine reduction that involves a proton abstraction from an Fe(II)-bound amine to yield Fe(III)(RNH)^- species. These amine chelates then react with water to form the iron oxide, still containing the amine surfactant at the surface. One of the advantages of the amine matrix is that the hydrolysis of the metal ion is accelerated in its presence and it occurs readily without the addition of a base because amine provides the basic media.¹⁹ On the basis of these facts, we may conclude that amine acts as a reductant in a N_2 atmosphere and Fe_3O_4 may originate from the $\text{Fe}^{2+/3+}$ chelates reduced by amine with the oxygen originating from the OH ligands. A thermogravimetric analysis (TGA) of the magnetite nanoparticles obtained after drying the colloidal solution was performed over the temperature range 20–600 °C in a nitrogen atmosphere. TGA of DDA-coated Fe_3O_4 nanoparticles indicates chemisorption of DDA at the nanoparticle surface and its multilayer deposition at higher DDA concentration (1:7 Fe:amine mole ratio). The first and brief event of weight loss occurs around 100 °C and is due to evaporation of the adsorbed solvent. The TGA data (Figure 3A) demonstrated that regardless of the atmosphere, the major mass loss in DDA-coated nanoparticles

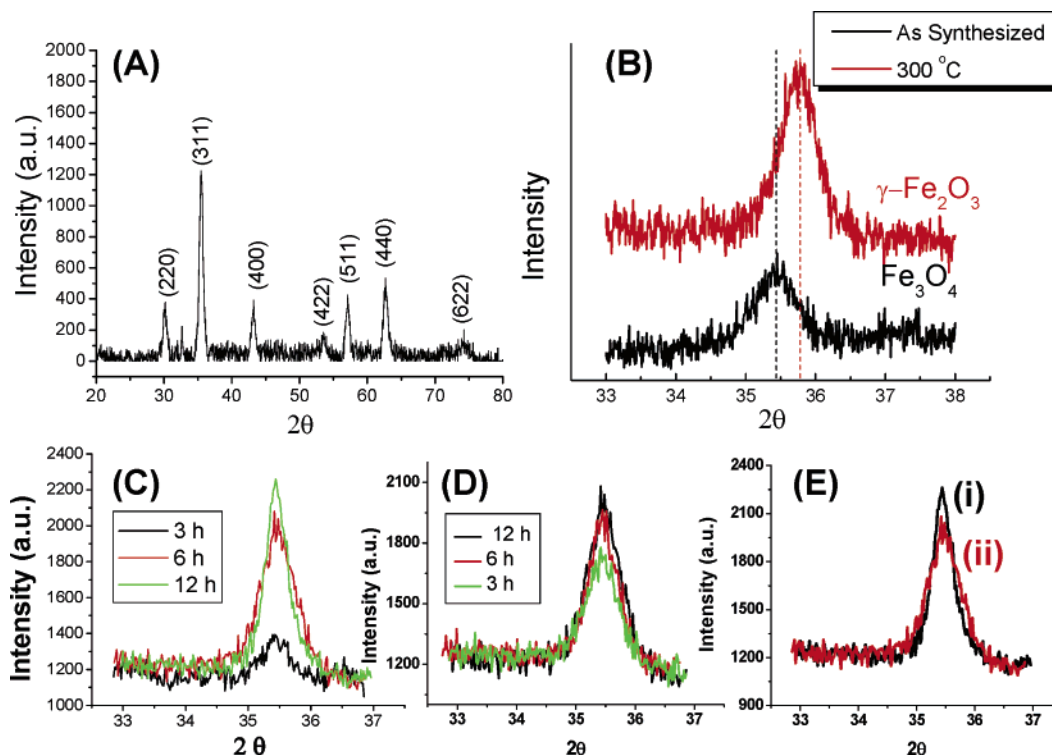


Figure 2. (A) X-ray diffraction scan iron oxide nanoparticles produced with a 1:1 Fe:amine mole ratio; (B) superimposed XRD patterns (slow scan, 0.01°/step) of as-synthesized (1:1 Fe:amine) and annealed sample (300 °C) indicating the peak shift to the formation of the γ -Fe₂O₃ phase. (C) Main peak XRD scans for a 1:4 Fe:amine mole ratio and (D) a 1:7 Fe:amine mole ratio. Three different curves in C and D indicate the kinetic growth of nanoparticles at 3, 6, and 12 h. (E) Superimposed XRD patterns of nanoparticles after 12 h of reaction time for (i) a 1:4 Fe:amine mole ratio and (ii) a 1:7 Fe:amine mole ratio.

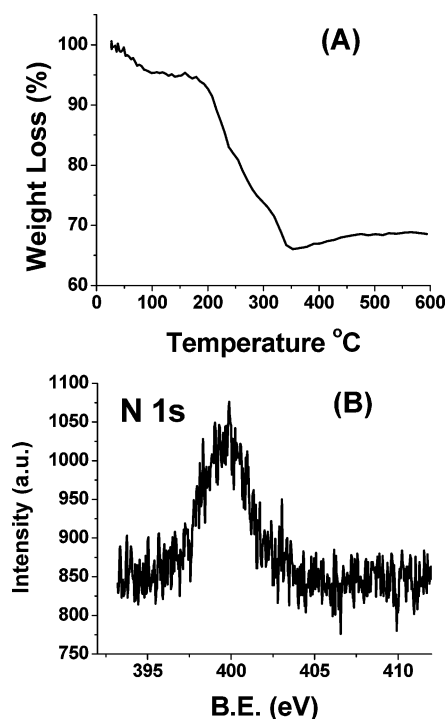


Figure 3. (A) Thermogravimetric plot of iron oxide nanoparticles produced with a 1:7 Fe:amine mole ratio, and (B) N 1s XPS spectrum of corresponding dried nanoparticle powder.

occurs between the range 210–350 °C, which is higher than that for the pure DDA (248 °C, bp). This shift in the temperature could be due to multilayered adsorption of DDA on the iron oxide surface, requiring higher temperature for the vaporization of bound DDA. This is followed by a minor weight gain between 350 and 450 °C. Perhaps this complex behavior results from the protective nature

of amine molecules on the iron oxide surface, which distinguishes quite well the dehydration of the magnetite powder and ultimately causes very slow and delayed oxidation of Fe²⁺ around 300 °C. The transformation of magnetite into maghemite corresponds to the feature at around 200 °C.²⁰ This is reported for DTA/TGA experiments conducted on maghemite: no feature is observed on any curves except the weight loss due to dehydration of powders.²⁰ We believe that the amine monolayer protects the magnetite structure well, and hence, there is no competition between dehydration and oxidation of Fe²⁺, as had been seen earlier for magnetite structures.²¹ The final phase transformation of maghemite into hematite is observed at around 500 °C.²²

FTIR of amine-functionalized Fe₃O₄ particles further supports the chemisorption of DDA and is especially valuable for confirming the expected presence of distinctive vibrations due to the presence of amine on the particles. FTIR spectra of the DDA precursor and DDA-Fe₃O₄ nanoparticles are shown in the Supporting Information (Figure S2, superimposed and magnified view, respectively), and selected band assignments are indicated. The spectrum of DDA is similar to the published spectrum.²³ The peak at 3325 cm⁻¹, which corresponds to the N–H stretching vibration mode, appears very weak and shifts to lower wave number when the DDA molecules adsorb on the nanoparticle surface, giving strong evidence that DDA anchors on the iron oxide surface through the N atom of the amine group in DDA. From the XPS measurements, Fe 3p_{3/2} and Fe 3p_{1/2} peaks observed at 711.0 and 724.8 eV, respectively, were identified with DDA-Fe₃O₄ nanoparticles (see the Supporting Information, Figure S3).²⁴ Fe, N, and O peaks are corrected with reference to the C 1s peak at 284.5 eV. A symmetric N 1s peak for Fe₃O₄-DDA nanoparticles appears at 400.0 eV, indicating the presence of N as a charged species (Figure 3B). If there is a contribution from the iron amine complex, a very low intensity peak at 397.3 eV appears.²⁵ The BE region corresponding to the free amine group or bonded amine falls in the range 398–400 eV. This peak suggests the involvement of electrostatic interactions, particularly with a nanoparticle surface, and is in agreement with earlier observations.²⁶

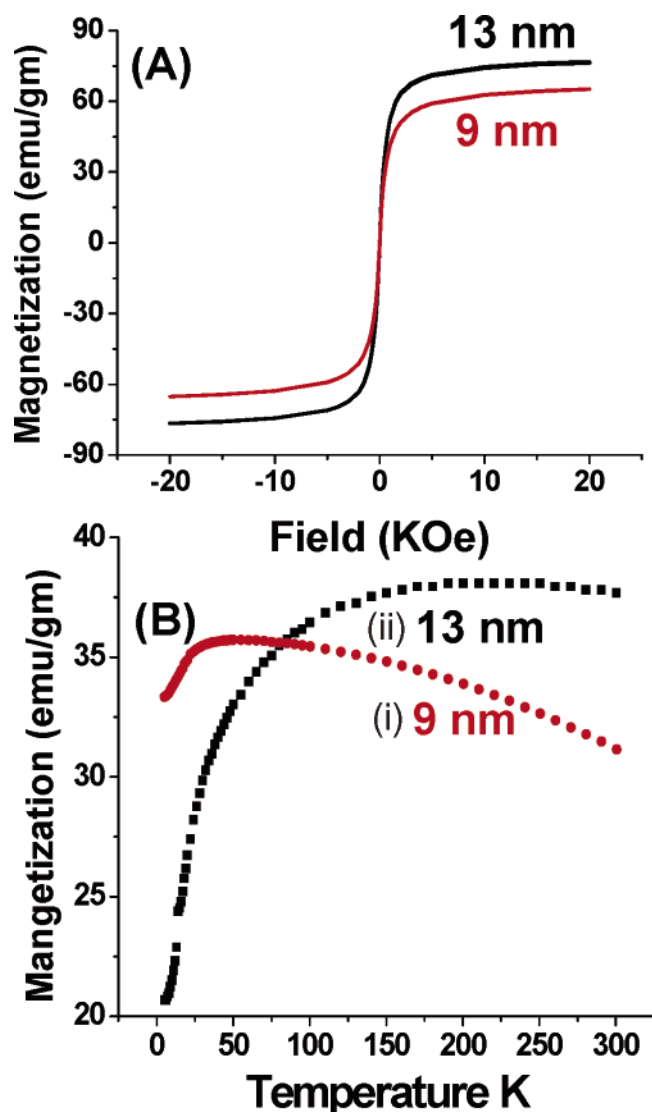


Figure 4. (A) Superimposed hysteresis curves for 9 and 13 nm DDA- Fe_3O_4 nanoparticles prepared with 1:4 and 1:7 Fe:amine mole ratios. (B) ZFC curves of respective nanoparticles. The field applied for magnetization was 500 Oe.

Figure 4A shows the room-temperature hysteresis magnetization of dried magnetite nanoparticles obtained by SQUID magnetometry. Both 9 and 13 nm DDA- Fe_3O_4 nanoparticles exhibit superparamagnetic characteristics, indicating that the thermal energy can overcome the anisotropy energy barrier of a single particle and that the net magnetization of the particle assemblies in the absence of an external magnetic field is zero. The saturation magnetization was 60 and 70 emu/g for 9 and 13 nm size particles, respectively. The difference in saturation magnetization of the samples is mainly attributed to the differences in particle size. In addition, saturation magnetizations of our samples are slightly lower than those of similarly sized nanoparticles prepared by other methods,²⁷ which might be caused by the surface spin-canting effects created by the amine molecule on the nanoparticle surface.²⁸ Figure 4B shows the zero-field-cooling curves of 9 and 13 nm particles. Curve (i)

decreases rapidly with temperature and suggests that 9 nm particles are superparamagnetic with little interaction among the particles.²⁹ Curve (ii) decreases slowly with temperature and indicates that 13 nm particles are superparamagnetic with some interactions among the particles.

With respect to the preparation of amine-capped magnetite nanoparticles, the amine plays an important role in the reaction process. DDA did not dissolve in water at room temperature, but the reaction proceeded immediately after 35 °C was reached, affording a highly dispersive liquid of Fe_3O_4 nanoparticles in a short time. On the other hand, the DDA molecules did not react with FeCl_2 at 100 °C, and they phase-separated as an oily layer. This suggests that the intermediate Fe(II)-amine complex is stable in the aqueous condition and that its reactivity strongly depends on the nature of the amine, indicating that the iron oxide nanoparticles are produced via the Fe(II)-amine complex with the first step and that the second step is its thermal decomposition. Thus, thermal decomposition of the Fe(II)-amine complex formed in water was so rapid that the Fe_3O_4 nanoparticles were subsequently strongly protected by the multilayers of amine molecule to avoid aggregation of nanoparticles. In practice, the particle size was influenced by the reaction time. Therefore, particle size is determined by thermal decomposition of the Fe(II)-amine complex formed in aqueous condition and is affected by changing the amine concentration. A similar reaction was reported for the preparation of iron oxide nanoparticles by the reaction of Fe-acetylacetonate ($\text{Fe}(\text{acac})_3$) and 2-pyrrolidone at high temperature.¹⁴

The effect new nanoparticles have on the magnetic relaxation of water protons in tissues (relaxivity) is an important property for use as MRI contrast agents. The transverse relaxivity (r_2), defined as the slope of $1/T_2$ vs mM Fe) was determined for the DDA- Fe_3O_4 nanoparticles. Transverse relaxation times (T_2) were measured at 60 MHz and 37 °C using both Carr-Purcell-Meiboom-Gill (CPMG) and spin-echo pulse sequences. The r_2 values for the reaction conditions measured are shown in Table 1. During the relaxivity experiment, the T_2 relaxation times at higher iron concentrations were stable over time at 37 °C, whereas at lower concentrations, the relaxation times became longer over time. The relaxivity values reveal no apparent trend in regards to reaction time or Fe:amine molar ratio, but further investigation is needed.

The colloid stability and biocompatibility of nanoparticles is of great importance. To investigate the effects of buffer, pH, and ionic strength on the DDA- Fe_3O_4 nanoparticles, we exposed them to buffered solutions of phosphate, citrate, acetate, MOPS, HEPES, and Tris. The buffered solutions were in the pH range of 5–8 and ion strength was adjusted using 0–500 mM NaCl. Although the DDA- Fe_3O_4 particles showed excellent stability in pure water, the stability in buffered solutions was surprisingly low. DDA- Fe_3O_4 particles synthesized with reaction times of 3 h were tested in Tris pH 7 and pH 8 while the reaction was incomplete (reaction 1, 1:1, 3 h reaction time; reaction 2, 1:4, 3 h reaction time); however the particles completely precipitated within 18 h. DDA- Fe_3O_4 particles from reaction 2 (1:4, 12 h reaction time) were found to be stable in sodium acetate pH 5, Tris pH 7, and Tris pH 8 for at least 3 weeks, whereas in other buffered conditions, the nanoparticles either immediately precipitated upon addition or completely precipitated within several hours. Particles from reaction 1 B (1:1 ratio, 12 h reaction time) were stable in Tris pH 7 and Tris pH 8 for 8 days before minimal precipitation began to occur.

Table 1. Relaxivity and Hydrodynamic Size of DDA- Fe_3O_4 Nanoparticles

reaction conditions (Fe:amine molar ratio; reaction time)	CPMG r_2 ($\text{mM}^{-1}\text{s}^{-1}$)	correlation coeff	spin-echo r_2 ($\text{mM}^{-1}\text{s}^{-1}$)	correlation coeff	hydrodynamic size (nm)
1:1; 3 h	177	0.9946	173	0.9942	1000
1:1; 12 h	87	0.9975	80	0.9954	29
1:4; 3 h	213	0.9937	212	0.9964	33
1:4; 12 h	141	0.9995	137	0.9982	31
1:7; 12 h	233	0.9997	232	0.9994	39

The hydrodynamic size of the colloidal suspension was obtained using dynamic light scattering (DLS) and is shown in Table 1. These data corroborate TEM measurements showing that reaction 1 (3 h) yields nanoparticles that are an agglomerated mixture of rodlike and spherical particles. The other three conditions yield nanoparticles that are spherical and more monodispersed. For comparison, dextran-coated cross-linked iron oxide nanoparticles were investigated. The r_2 for the dextran-coated particles was found to be $\sim 113 \text{ mM}^{-1} \text{ s}^{-1}$ and the hydrodynamic size was $\sim 25 \text{ nm}$. When particles are more uniform in size (reactions 1B and 1C), the DDA-Fe₃O₄ particles have a relaxivity ~ 2 times higher than the dextran-coated particles, but have similar hydrodynamic sizes.

In conclusion, the synthesis reported here is a novel reaction, affording uniform magnetite nanoparticles capped by amine ligands from a single precursor FeCl₂ that renders amine-capped water-dispersible particles. The results indicate that higher DDA concentrations and longer reaction times lead to more stable, monodisperse nanoparticles with high relaxivity for use in biomedical applications. We are currently investigating these particles with DNA linkages and cell viability, as amine is a “backbone functional group” in biological molecules.

Acknowledgment. This research was supported by the Center for Cancer Nanotechnology Excellence (CCNE) initiative of the National Institutes of Health’s National Cancer Institute under Award U54CA119341. Any opinions, findings, and conclusions or recommendations expressed in this material are those of the author(s) and do not necessarily reflect those of the National Institutes of Health. This work was performed in the EPIC/NIFTI facility of the NUANCE centre (supported by NSF-NSEC, NSF-MRSEC, Keck Foundation, the State of Illinois, and Northwestern University) at Northwestern University.

Supporting Information Available: TEM data, XRD patterns, FTIR spectroscopy, and XPS data. This material is available free of charge via the Internet at <http://pubs.acs.org>.

References

- Raj, K.; Moskowitz, B.; Casciari, R. *J. Magn. Magn. Mater.* **1995**, *149*, 174.
- Sun, S.; Weller, D. *J. Magn. Soc. Jpn.* **2001**, *25*, 1434.
- Weller, D.; Moser, A. *IEEE Trans. Magn.* **1999**, *35*, 4423.
- Weiss, W.; Ranke, W. *Prog. Surf. Sci.* **2002**, *70*, 1.
- Wu, P. G.; Zhu, J. H.; Xu, Z. H. *Adv. Funct. Mater.* **2004**, *14*, 345.
- Mohri, K.; Uchiyama, T.; Panina, L. V. *Sens. Actuators, A* **1997**, *59*, 1.
- Rossi, L. M.; Quach, A. D.; Rosenzweig, Z. *Anal. Bioanal. Chem.* **2004**, *380*, 606.
- Levy, L.; Sahoo, Y.; Kim, K. S.; Bergey, E. J.; Prasad, P. N. *Chem. Mater.* **2002**, *14*, 3715.
- Huh, Y. M.; Jun, Y. W.; Song, H. T.; Kim, S.; Choi, J. S.; Lee, J. H.; Yoon, S.; Kim, K. S.; Shin, J. S.; Suh, J. S.; Cheon, J. *J. Am. Chem. Soc.* **2005**, *127*, 12387.
- Song, H. T.; Choi, J. S.; Huh, Y. M.; Kim, S.; Jun, Y. W.; Suh, J. S.; Cheon, J. *J. Am. Chem. Soc.* **2005**, *127*, 9992.
- Kang, Y. S.; Risbud, S.; Rabolt, J. F.; Stroeve, P. *Chem. Mater.* **1996**, *8*, 2209. (b) Hong, C.-Y.; Jang, I. J.; Horng, H. E.; Hsu, C. J.; Yao, Y. D.; Yang, H. C. *J. Appl. Phys.* **1997**, *81*, 4275. (c) Sapieszko, R. S.; Matijevic, E. *J. Colloid Interface Sci.* **1980**, *74*, 405.
- (a) Sun, S.; Zeng, H. *J. Am. Chem. Soc.* **2002**, *124*, 8204. (b) Sun, S.; Zeng, H.; Robinson, D. B.; Raoux, S.; Rice, P. M.; Wang, S. X.; Li, G. *J. Am. Chem. Soc.* **2004**, *126*, 273.
- Park, J.; An, K.; Hwang, Y.; Park, J.-G.; Noh, H.-J.; Kim, J.-Y.; Park, J.-H.; Hwang, N.-M.; Hyeon, T. *Nat. Mater.* **2004**, *3*, 891–895.
- Li, Z.; Chen, H.; Bao, H.; Gao, M. *Chem. Mater.* **2004**, *16* (8), 1391–1393.
- A quantity of 100 mL of a 10 mM concentrated aqueous solution of ferrous chloride (FeCl₂·4H₂O) was reduced by 40 mM dodecyl amine under mild heating at 85 °C to yield stable iron oxide nanoparticles in water. Although the mixture turns black immediately after mixing, indicating that nanoparticles are produced by the room temperature reaction of amine with FeCl₂, we have observed that the rate of reduction of Fe²⁺ ions by amine is considerably enhanced around the boiling point of water and, consequently, all nanoparticle syntheses were carried out at this temperature. The amine-reduced iron oxide nanoparticle solution was subjected to magnetic separation, and the resulting aggregate was washed with copious amounts of acetone and deionized water to remove any uncoordinated amine molecules. The aggregate was then redispersed in deionized water for further studies.
- Josephson, L.; Tung, C. H.; Moore, A.; Weissleder, R. *Bioconjugate Chem.* **1999**, *10*, 186.
- Hyeon, T.; Lee, S. S.; Park, J.; Chung, Y.; Na, H. B. *J. Am. Chem. Soc.* **2001**, *123*, 12798–12801.
- (a) Hostetler, M. J.; Wingate, J. E.; Zhong, C. J.; Harris, J. E.; Vachet, R. W.; Clark, M. R.; Londono, D. J.; Green, S. J.; Stokes, J. J.; Wignall, G. D.; Glish, G. L.; Porter, M. D.; Evans, N. D.; Murray, R. W. *Langmuir* **1998**, *14*, 17. (b) Chen, S.; Murray, R. W. *Langmuir* **1999**, *15*, 682. (c) Motte, L.; Pileni, M. P. *J. Phys. Chem. B* **1998**, *102*, 4104. (d) Micic, O. I.; Ahrenkiel, S. P.; Nozik, A. Z. *Appl. Phys. Lett.* **2001**, *78*, 4022.
- Kandori, K.; Yasukawa, A.; Ishikawa, T. *J. Colloid Interface Sci.* **1996**, *180*, 446.
- Cornell, R. M.; Schwertmann, U. *The Iron Oxides*; VCH: New York, 1996; p 135.
- Daou, T. J.; Pourroy, G.; Begin-Colin, S.; Greneche, J. M.; Ulhaq-Bouillet, C.; Legare, P.; Bernhardt, P.; Leuvre, C.; Rogez, G. *Chem. Mater.* **2006**, *18* (18), 4399–4404.
- Xisheng, Y.; Dongsheng, L.; Zhengkuan, J.; Lide, Z. *J. Phys. D: Appl. Phys.* **1998**, *31*, 2734.
- Puchert, C. J. *The Aldrich Library of FT-IR Spectra*, 2nd ed.; Sigma-Aldrich: Milwaukee, WI, 1997; Vol. 1, p 506.
- (a) Teng, X. W.; Black, D.; Watkins, N. J.; Gao, Y. L.; Yang, H. *Nano Lett.* **2003**, *2*, 261. (b) McIntyre, N. S.; Zetaruk, D. G. *Anal. Chem.* **1977**, *49*, 1521.
- (a) Wu, J. B.; Lin, Y. F.; Wang, J.; Chang, P. J.; Tasi, C. P.; Lu, C. C.; Chiu, H. T.; Yang, Y. W. *Inorg. Chem.* **2003**, *42*, 4516. (b) Charlier, J.; Cousty, J.; Xie, Z. X.; Poulennec, V. L.; Bureau, C. *Surf. Interface Anal.* **2000**, *30*, 283.
- Sharma, J.; Mahima, S.; Kakade, B. A.; Pasricha, R.; Mandale, A. B.; Vijayamohan, K. *J. Phys. Chem. B* **2004**, *108* (35), 13280–13286.
- Sun, S. H.; Zeng, H. *J. Am. Chem. Soc.* **2002**, *124*, 8204.
- (a) Vestal, R.; Zhang, Z. *J. Am. Chem. Soc.* **2003**, *125*, 9828. (b) Morales, M. P.; Veintemillas-Verdaguer, S.; Montero, M. I.; Serna, C. J.; Roig, A.; Casas, L.; Martinez, B.; Sandiumenge, F. *Chem. Mater.* **1999**, *11*, 3058.
- Bodker, F.; Hansen, M. F.; Koch, C. B.; Lefmann, K.; Morup, S. *Phys. Rev. B* **2000**, *61*, 6826.

CG060656P